Red Sea Rifting Controls on Groundwater Reservoir Distribution: Constraints from Geophysical, Isotopic, and Remote Sensing Data

CONFERENCE PAPER · OCTOBER 2008

READS
15

9 AUTHORS, INCLUDING:

Neil C Sturchio
University of Delaware
324 PUBLICATIONS **6,950** CITATIONS
SEE PROFILE

Richard H Becker
University of Toledo
109 PUBLICATIONS **572** CITATIONS
SEE PROFILE

Jay Sagin
Nazarbayev University
27 PUBLICATIONS **54** CITATIONS
SEE PROFILE

Mohamed Ahmed
Western Michigan University
76 PUBLICATIONS **53** CITATIONS
SEE PROFILE

Red Sea rifting controls on aquifer distribution: Constraints from geochemical, geophysical, and remote sensing data

M. Sultan[1,†], A.F. Yousef[2], S.E. Metwally[2], R. Becker[3], A. Milewski[1], W. Sauck[1], N.C. Sturchio[4], A.M.M. Mohamed[5], A. Wagdy[6], Z. El Alfy[7], F. Soliman[8], M. Rashed[8], D. Becker[1], Z. Sagintayev[1], M. Ahmed[1], and B. Welton[1]

[1]*Department of Geosciences, Western Michigan University, Kalamazoo, Michigan 49008-5200, USA*
[2]*Desert Research Center, El Matariya, Cairo, Egypt*
[3]*Department of Environmental Sciences, University of Toledo, Toledo, Ohio 43606, USA*
[4]*Department of Earth and Environmental Sciences, University of Illinois at Chicago, Chicago, Illinois 60607-7059, USA*
[5]*Department of Geology, South Valley University, Qena, Egypt*
[6]*Irrigation and Hydraulics Engineering Department, Cairo University, Giza, Egypt*
[7]*Hammash Misr for Gold Mines, Cairo, Egypt*
[8]*Department of Geology, Suez Canal University, Ismalia, Egypt*

ABSTRACT

Highly productive wells in the Central Eastern Desert of Egypt are tapping groundwater in subsided blocks of Jurassic to Cretaceous sandstone (Taref Formation of the Nubian Sandstone Group) and Oligocene to Miocene sandstone (Nakheil Formation), now occurring beneath the Red Sea coastal plain and within the proximal basement complex. Aquifer development is related to Red Sea rifting: (1) rifting was accommodated by vertical extensional displacement on preexisting NW-SE– to N-S–trending faults forming a complex array of half-grabens and asymmetric horsts; and (2) subsided blocks escaped erosion accompanying the Red Sea–related uplift. Subsided blocks were identified and verified using satellite data, geologic maps, and field and geophysical investigations. Interpretations of very low frequency (VLF) measurements suggest the faults acted as conduits for ascending groundwater from the subsided aquifers. Stable isotopic compositions (δD: –19.3‰ to –53.9‰; δ^{18}O: –2.7‰ to –7.1‰) of groundwater samples from these aquifers are interpreted as mixtures of fossil (up to 70%) and modern (up to 65%) precipitation. Groundwater volumes in subsided blocks are large; within the Central Eastern Desert basement complex alone, they are estimated at 3×10^9 m^3 and 10×10^9 m^3 for the Nakheil and Taref Formations, respectively. Results highlight the potential for identifying similar rift-related aquifer systems along the Red Sea–Gulf of Suez system, and in rift systems elsewhere. An understanding of the distribution of Red Sea rift–related aquifers and modern recharge contributions to these aquifers could assist in addressing the rising demands for fresh water supplies and water scarcity issues in the region.

INTRODUCTION

Countries in the arid and semiarid parts of the world are facing shortages in their fresh water supplies because of their increasing populations and the absence of a comprehensive understanding of the geologic and hydrogeologic controls on the development and preservation of these resources. Such an understanding is needed to enable sustainable utilization of these resources. One such area is the Saharan Africa and the Middle Eastern countries. A vital resource for the populations of some of these countries is the extensive system of rivers that collect precipitation from distant mountainous areas and channel it from regions where precipitation is abundant to the much drier climatic regions downstream. One such system is the Nile River watershed that collects precipitation from the highlands in subtropical Africa and channels it to Saharan Africa. Unfortunately, the majority of the world's arid and semiarid regions lack extensive river systems and must resort to other freshwater resources. Many of the arid and semiarid parts of the world are fortunate in having large amounts of fresh water stored in extensive aquifers that stretch for hundreds to thousands of kilometers across political boundaries; these are largely nonrenewable aquifers, commonly referred to as "fossil" aquifers. Fossil aquifers are believed to have been recharged under previous wet climatic periods (e.g., Sturchio et al., 2004) but may have also received local meteoric contributions in intervening dry climatic periods (such as at present; Sultan et al., 2007, 2008a). These aquifers are of extreme importance to the general population of these countries given the prevailing arid conditions and the increasing need for fresh-water supply in these areas. The identification of the hydrologic and geologic settings of these groundwater resources, the assessment of their areal distribution, and the understanding of the modern contributions to these systems could assist in addressing water shortage problems in these areas. In this paper, we examine one such setting, namely aquifers in the Red Sea rift system.

An integrated approach, involving data from field, geochemical, geophysical, and remote sensing and geographic information system (GIS) studies, was applied to identify the distribution of the Red Sea–related extensional structures and aquifers and to assess their groundwater potential on a regional scale. The role of these structures in aquifer development, groundwater transport, and groundwater exchange between aquifers is examined. We also identify the origin of groundwater in these structurally controlled aquifers and examine potential mechanisms for groundwater recharge.

GEOLOGIC SETTING

The Red Sea began to open about 20 million years ago during the late Oligocene to early Miocene as the Red Sea rift propagated northward

[†]E-mail: mohamed.sultan@wmich.edu

GSA Bulletin; May/June 2011; v. 123; no. 5/6; p. 911–924; doi: 10.1130/B30146.1; 8 figures; 2 tables.

and separated the Arabian plate from the once-contiguous Arabian-Nubian plate (Bosworth et al., 2005) (Fig. 1). Rifting was associated with uplift; the shoulders of the rift along the Red Sea and the Gulf of Suez and along the Dead Sea transform fault were elevated by as much as 4 km, exposing the underlying crystalline rock and the overlying thick (up to 2.5 km) sedimentary successions to extensive erosion (Garfunkel and Bartov, 1977). The rifting was largely accommodated by extensional normal faults that strike north and northwest forming a complex array of half-grabens and asymmetric horsts (Pivnik et al., 2003) (Fig. 1). Whereas the uplift devastated the thick sedimentary successions (largely Eocene limestone and Cretaceous sandstone), the extensional faults preserved these successions as subsided blocks under the Red Sea and Gulf of Suez coastal plains and the Red Sea trough. Fossil groundwater from subsided Cretaceous Nubian Sandstone blocks

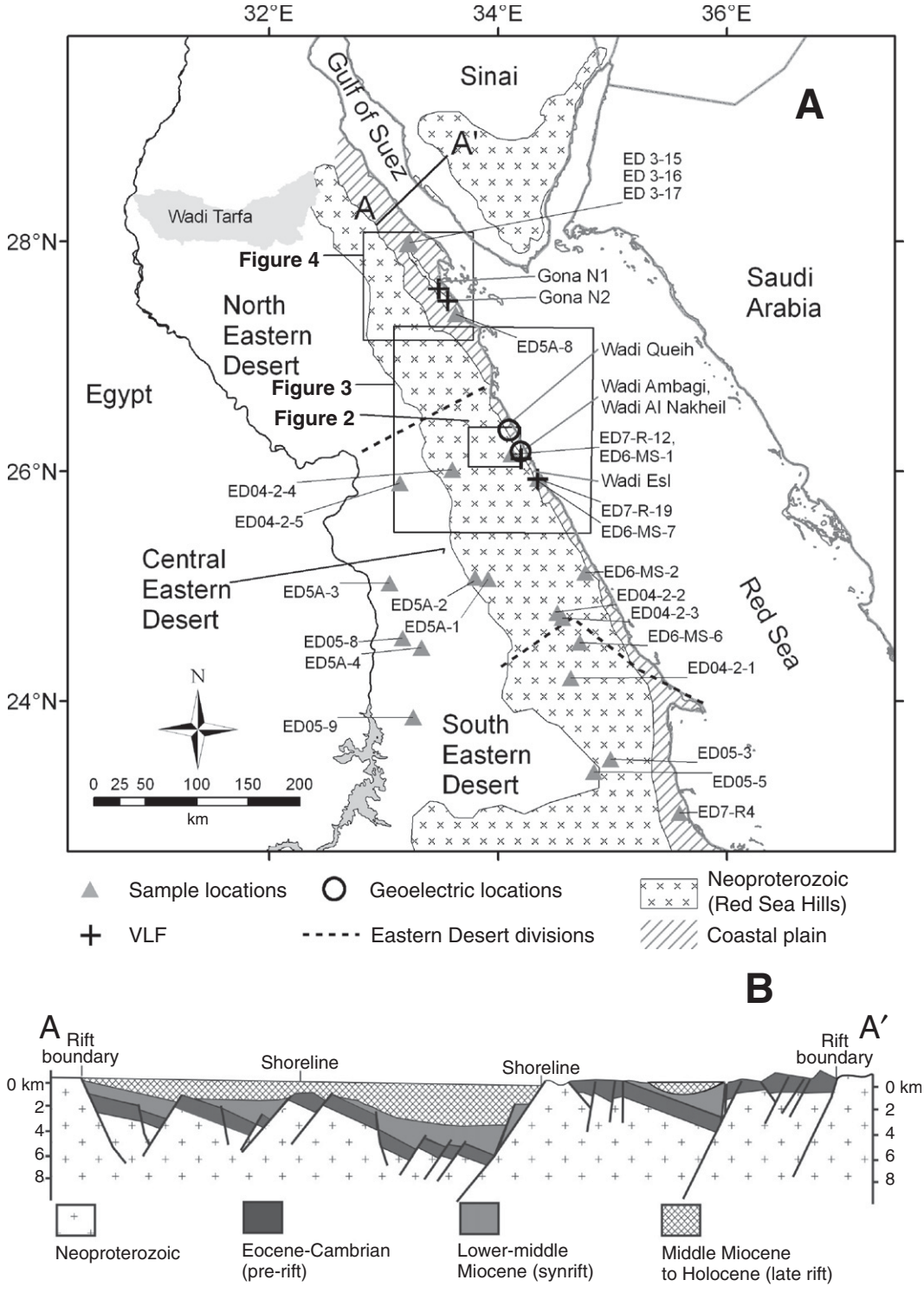

Figure 1. (A) Location map showing the distribution of Neoproterozoic outcrops along the Red Sea margins, the Red Sea coastal plain, and the lithotectonic subdivisions of the Eastern Desert (Stern, 1985). Also shown are the locations of our groundwater samples, geoelectric cross sections in Wadis Queih and Al Nakheil, and very low frequency (VLF) transects in Wadis Esl and Ambagi, Gona North-1, and Gona North-2 areas. (B) Simplified cross section along line A–A′ in Figure 1A modified from Pivnik et al. (2003). Areas covered by Figures 2, 3, and 4 are outlined by boxes.

(up to 4 km deep) discharges along the extensional faults bounding the Gulf of Suez at high temperature (up to 70 °C) within the coastal plain of the Gulf of Suez and along its coastline (Sturchio et al., 1996). In Sinai, these fossil waters originated as precipitation over the mountains of southern Sinai, and recharged the aquifers cropping out at the foothills. The groundwater flow directions are northward, toward the Mediterranean Sea, and westward toward the Gulf of Suez (west) where discharge occurs along the faults defining the Gulf (Issar, 1979). These extensional faults are not restricted to the Red Sea and Gulf of Suez coastal plains and trough but extend inland affecting the basement complex proximal to the coastal plain. There are numerous subsided sedimentary successions, now preserved as subsided blocks within the basement complex (Klitzsch et al., 1987a, 1987b, 1987c, 1987d, 1987e, 1987f).

Inspection of Figure 1B, a cross section along line A–A′ in Figure 1A, indicates that the general stratigraphic and structural elements of the coastal plain are similar to, and continuous with, the structures and lithologies that define the Gulf of Suez rift. Within the rift and the coastal plain domains, southwest-dipping normal faults and northeast-dipping bedding characteristic of the central part of the rift are observed. These dip directions (or polarities) reverse at intervals along the strike of the Red Sea–Gulf of Suez rift; the zones having opposite dips are separated by broad transverse accommodation zones (Younes and McClay, 2002), also termed transfer zones (Moustafa, 2002) or hinge zones (AlSharhan, 2003).

The stratigraphy of the Gulf of Suez area and the Red Sea has been reviewed by Abdel-Gawad (1970), Reynolds (1979), Wasfi and Azazi (1979), Winn et al. (2001), and Moustafa (2002). The sedimentary successions to the west and east of the Red Sea Hills along its coastal plain are similar to those observed in the Gulf of Suez. They are grouped into two main groups: (1) pre-rift Cambrian–Eocene and (2) synrift post-Eocene, largely Miocene, successions. Unconformably overlying the Precambrian basement is a section of Carboniferous through Eocene sedimentary rocks (shale, sandstone, and limestone). A porous Jurassic to Upper Cretaceous age rock unit, commonly referred to as the Nubian Sandstone Group, has good hydrologic aquifer properties and is overlain by a sequence of Upper Cretaceous through Upper Eocene limestone, dolostone, shale, chalk, and marl, which acts as a confining layer to the underlying Nubian Sandstone. A major unconformity separates the pre-Miocene sediments (pre-rift succession) from the overlying younger deposits (synrift succession). The uplift was followed by a period of intense extension and faulting along axes trending NW-SE, NNW-SSE, and N-S.

VERTICAL DISPLACEMENT ON PREEXISTING ACCRETIONARY AND POSTACCRETIONARY PLANES OF WEAKNESS

Studies have shown that for the Red Sea rift system and surrounding areas in the Afar region, it is easier to propagate extensional displacement along preexisting faults than to develop new faults, especially for those oriented at near right angles to the least compressive stress directions (Dixon et al., 1987; Korme et al., 2004). In the Eastern Desert, these correspond to the N-S–trending accretionary fold and thrust belt structures and the postaccretionary NW-oriented Najd faults and shears. The Najd shear system extends over 1200 km in a NW-SE direction in the Arabian Shield, with an average width of ~300 km (Agar, 1987). It aligns with faults in the South Yemen coast and in the Arabian seafloor to the SE (Brown and Coleman, 1972), making a potential total length in excess of 2000 km (Moore, 1979). Using a pre–Red Sea rift reconstruction, together with field, geochemical, and geochronological data, Sultan et al. (1988, 1992, 1993) mapped the extension of the Najd shear system of the Arabian Shield into the Central Eastern Desert of Egypt, bringing the total length of the Najd system in the Arabian and Nubian shields to 2300 km. Along the zone occupied by the Najd system in the Arabian-Nubian Shield, brittle and ductile styles of deformation prevail, superimpose on, and obliterate earlier accretionary tectonic features. We demonstrate that reactivation of the accretionary and postaccretionary fault systems during the opening of the Red Sea has played an important role in preserving the pre-rift sedimentary successions within the basement complex and show that these sediments now host substantial amounts of fossil groundwater. Many of the inland subsided successions are present within the Central Eastern Desert, in the area where the Najd fault system propagated (Sultan et al., 1988).

The color composite shown in Figure 2A for the Duwi area (area outlined by the smallest box in Fig. 1) was generated using ratios of Landsat thematic mapper (TM) bands (5/4 × 3/4, 5/1, and 5/7) that are sensitive to the rock content of Fe-bearing aluminosilicates, spectrally opaque, and hydroxyl-bearing or carbonate-bearing minerals, respectively (Sultan et al., 1987, 1988, 1992). On these images, crystalline rocks rich in hydroxyl-bearing phases and opaque phases (e.g., serpentinites) appear in shades of red, rocks rich in Fe-bearing aluminosilicates (e.g., gabbros and mafic volcanics) appear in shades of blue, and rocks poor in Fe-bearing aluminosilicates, hydroxyl-bearing minerals, and opaque phases (e.g., granites) appear green. Carbonate-rich rocks (e.g., Eocene limestone and marl) appear in shades of yellow, and quartz-rich Nubian Sandstone appears in shades of green. An interpretation map was constructed (Fig. 2B) using our field data and published field relations (Abuzeid, 1994) together with the spatial distribution of lithologic units displayed in Figure 2A.

We adopted the following satellite-based criteria and field observations (Sultan et al., 1988) to map Najd faults and brittle/ductile shear zones (e.g., A–A′, B–B′ C–C′, and D–D′; Fig. 2): (1) presence of NW-trending lithologic discontinuities that are tens of meters (faults) to hundreds of meters (shear zones) wide; (2) left-lateral sense of displacement along the observed lithologic discontinuities as evidenced from the displacement of distinctive lithologies across discontinuities or by changes in direction of structural trends and outcrop patterns of distinctive lithologies as they approach the inferred fault or brittle shear zone; (3) subhorizontal, NW-trending mineral lineations, and variably dipping, NW-trending foliations, with local changes in attitude around large competent (e.g., granitic) bodies; (4) lithologic contacts are generally tectonic in nature and related to faulting with outcrop patterns exhibiting considerable fine-scale heterogeneity on the outcrop scale (meters to hundreds of meters); and (5) presence of trails of serpentinite along fault traces because serpentinite accommodates movement efficiently at low temperature (Raleigh and Paterson, 1965). For all the serpentinite-decorated shear zones that were identified from satellite data and visited in the field (e.g., B–B′ and C–C′; Fig. 2), lithologic contacts are tectonic, brittle styles of deformation (e.g., fractures and breccias) are dominant, and pervasive structural elements (e.g., mineral stretching lineations and bedding foliation) are absent. These field observations are consistent with experimental results showing that the presence of small amounts of serpentinite (as low as 10%) can dramatically reduce the strength of altered peridotitic rocks and promote faulting and brittle deformation (Escartin et al., 2001). The presence of these planes of weakness also could have facilitated subsequent vertical displacement related to Red Sea extension.

The following observations are consistent with extensional displacement along preexisting Najd faults and shear zones in the Duwi area: (1) a number of subsided blocks are bound by NW-trending faults, the same trends that are displayed by Najd-related faults and shear zones in the area (e.g., extensional faults a–a′ and b–b′ are

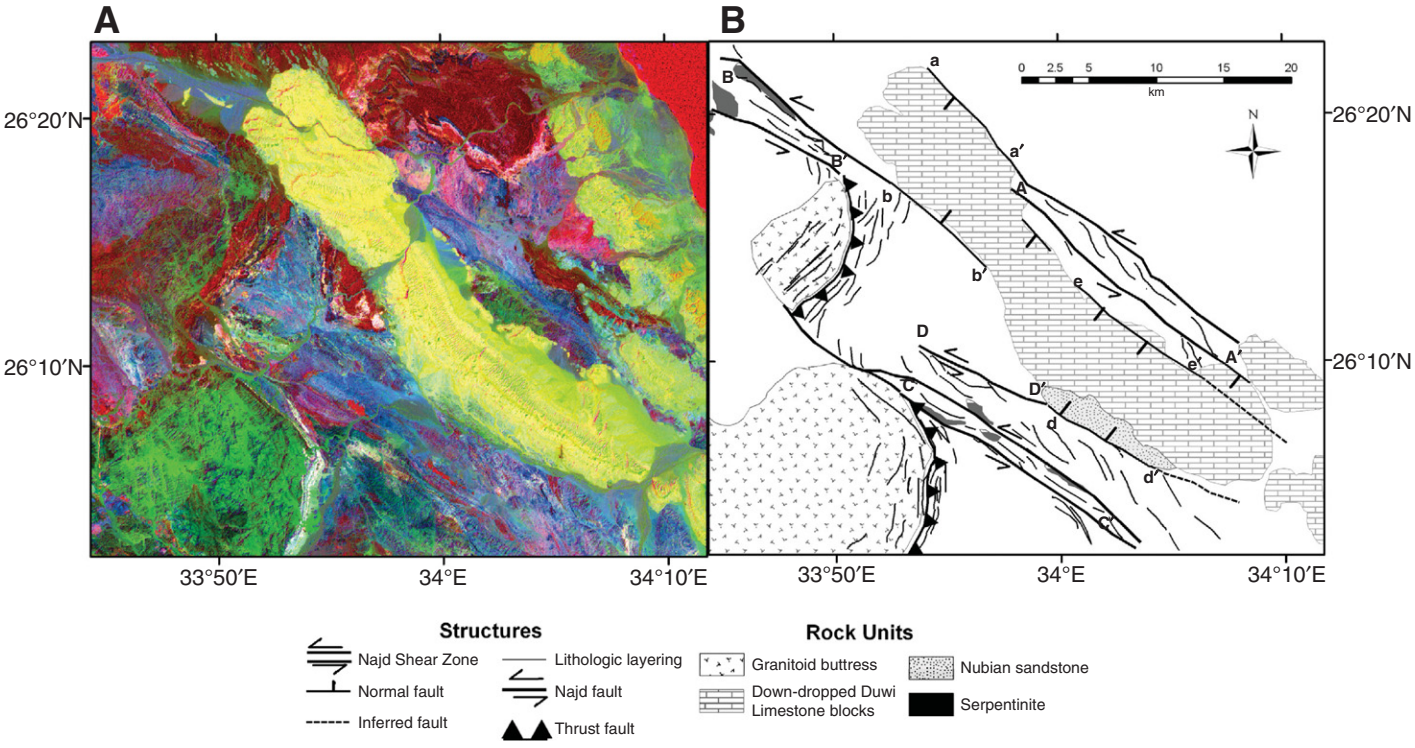

Figure 2. (A) Color composite of Landsat thematic mapper (TM) band ratios over the Duwi area and surroundings. The TM band 5/4 × 3/4 image is assigned the blue component, band 5/1 the green component, and band 5/7 the red component (modified from Sultan et al., 1993). (B) Interpretation map of Figure 2A showing the TM-based distribution of major extensional faults and Najd-related structural elements including major faults and shear zones and their inferred sense of displacement. Also shown are areas of recharge (e.g., Nubian Sandstone outcrops).

subparallel to the mapped Najd shear zones), and (2) a number of the extensional NW-trending faults that bound the subsided blocks lie along the postulated extension of Najd-related faults and shear zones. For example, the extensional faults a–a′ and b–b′ lie along the postulated extensions of the Najd shear zone A–A′ and B–B′, respectively, and the extensional fault D–D′ aligns with the Najd fault d–d′.

Not all of the subsided blocks within the basement complex were accommodated on preexisting NW-trending Najd structures. Some of them were apparently displaced along the N-S preexisting accretionary structures as well. Figure 3 shows the distribution of subsided sedimentary successions in sections of the Central Eastern Desert. These were outlined using geological, geophysical, and geochemical criteria outlined below. More subsided blocks are expected to be present beneath the coastal plain of the Gulf of Suez and the Red Sea.

METHODOLOGY AND FINDINGS

A regional integrated perspective was adopted to gain insights into the distribution of groundwater aquifers in subsided blocks and the groundwater potential of these subsided aquifers. This approach entailed the analysis of regional data sets including Bouguer gravity anomaly maps, remote sensing data, and geologic maps. A local integrated perspective that entailed the use of detailed field, geophysical, and geochemical data was adopted to investigate a number of critical issues: (1) vertical electrical sounding (VES) data were used to examine whether groundwater accumulations are to be found within the target rift-related aquifers that were selected using geological observations, remote sensing data, and regional gravity measurements; (2) VLF data were used to test whether extensional faults associated with Red Sea rifting could act as conduits for ascending groundwater from the subsided aquifers; and (3) stable isotope data (H and O isotope ratios within H_2O) were used to examine the origin of groundwater in these subsided aquifers and to constrain the timing and mechanisms of groundwater recharge.

The accomplishment of all of these tasks was facilitated through the integration of a number of coregistered data sets in a geographic information system (GIS) environment for a better understanding of the spatial interrelationships between relevant data sets. The integrated data sets were either of regional extent (e.g., geologic maps, Bouguer gravity anomaly map, and Landsat TM), or local extent (e.g., solute chemistry and resistivity).

Construction of a Web-Based GIS for Data Analysis and Visualization

The initial step in our methodology involved the generation of a database for data integration, analysis, and visualization. An Arc Info GIS-based interface for data manipulation and representation was generated to store and host the data sets via a web-based interface. The web-based interface was equipped with visualization routines to enable the analysis of the data in 2-D and 3-D environments. For the GIS, Oracle 9i was used as a database engine, and the database system was integrated with ArcGIS and Arc Internet Map Server (IMS) using Arc Spatial Database Engine (SDE) (Koeppel, 2001). We adopted the procedures and methodologies developed for the construction of the web-based GIS for Egyptian geological data sets and the web-based GIS for the Tethys belt (Sultan et al., 2003a, 2003b).

The database incorporates all relevant coregistered digital mosaics with a unified projection (Universal Transverse Mercator [UTM]

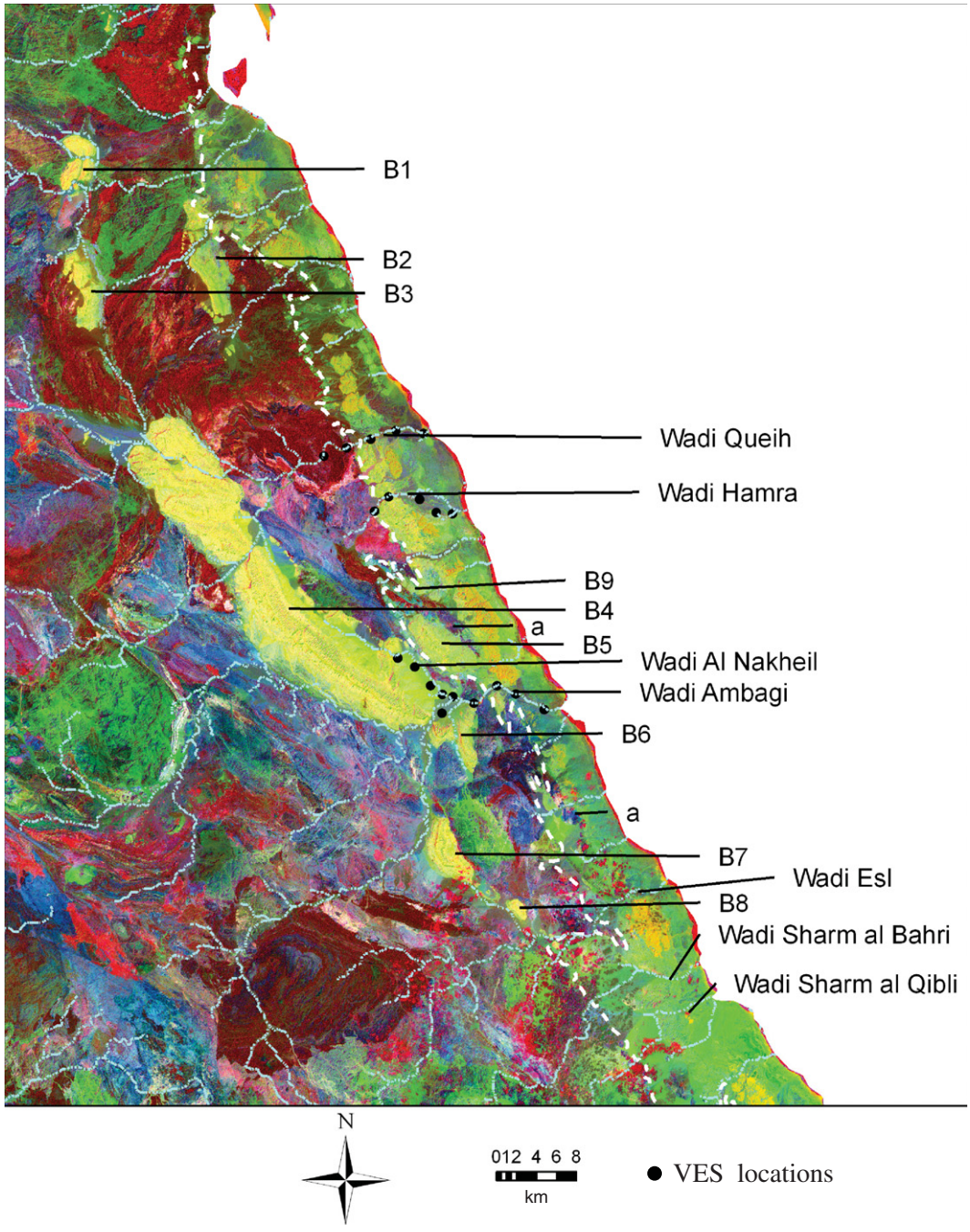

Figure 3. Distribution of subsided sedimentary successions (labeled "B1" through "B9") in the basement complex of the Central Eastern Desert and proximal to the coastal plain (area between white dotted line and the Red Sea). These were outlined using geological (e.g., distribution of pre-Miocene outcrops), geophysical (regional gravity and vertical electrical sounding [VES]), and geochemical (H_2O isotopic composition) criteria outlined in text. Also shown are the locations of (1) selected basement outcrops (labeled "a") within the coastal plain (outlined by dashed white line), and (2) selected stream networks and wadis and VES locations (black dots).

Zone 36) covering the Eastern Desert: (1) geologic maps (scale 1:500,000) (Klitzsch et al., 1987a, 1987b, 1987c, 1987d, 1987e, 1987f); (2) Bouguer anomaly gravity maps (scale 1:500,000) (Pohlmann and Deetz, 1987); (3) false-color mosaic of Landsat TM bands 2 (blue), 4 (green), and 7 (red) (spatial resolution: 28.5 m) created using processed individual reflectance TM bands; (4) Landsat TM band ratio mosaic (spatial resolution: 28.5 m) created using the Landsat TM reflectance band ratio mosaics (5/4 × 3/4, 5/1, and 5/7) (Sultan et al., 1987); (5) digital elevation models (DEMs; spatial resolution: 60 m) generated from raw Level 1A advanced spaceborne thermal emission and reflection radiometer (ASTER) scenes; (6) well data including one or more of the following parameters: well location, well name, well type, maximum drawdown, solute chemistry, total dissolved solids (TDS), H and O stable isotopic compositions, and depth to water table. Data were included for field samples from this study (Table 2; ~24 samples), field samples from our earlier studies (40 samples; Sultan et al., 2000, 2007), existing well data (~180 wells) administered by the Egyptian Ministry of Water Resources and Irrigation (EMWRI, 2004), and a compilation of well locations and names (up to 1995) extracted from topographic sheets (Egyptian General Survey Authority [EGSA], 1996a, 1996b, 1996c, 1996d, 1996e, 1996f, 1997a, 1997b, 1997c, 1997d, 1997e, 1997f); (7) resistivity data from subsided successions within the basement complex (Wadi Al Nakheil) and from others flooring the coastal plain (Wadi Queih); and (8) very low frequency (VLF) data acquired

TABLE 2. ISOTOPIC DATA FOR THE EASTERN DESERT GROUNDWATER SAMPLES FROM SUBSIDED BLOCKS, FRACTURED BASEMENT, AND PRODUCTIVE AND ARTESIAN WELLS TAPPING NUBIAN SANDSTONE

Field identification	Name	Latitude	Longitude	Well type and/or setting	DWT (m)	Temperature (°C)	$\delta^{18}O$ (‰)	δD (‰)	Origin
ED 3-15	Wadi Darah Sharm El Bahary	27.9758	33.2162	Open pit (LS*, S†)			–7.1	–52.0	F/M††
ED 3-16	Wadi Darah–Darah 4	27.9755	33.2047	(S†)			–7.1	–53.5	F/M††
ED 3-17	Wadi Darah–M.Abdul Aziz	27.9887	33.2283	Productive well (LS*, S†)			–7.1	–53.9	F/M††
ED5A-8	Gona	27.3670	33.6294	Productive well (S†)		~32	–6.2	–48.1	F/M††
ED6-MS-1	Wadi Ambagi	26.1053	32.2012	Spring (S†)	0		–4.6	–35.4	F/M††
ED6-MS-7	Wadi Esl 1	25.9327	34.3538	Productive well (S†)	>15 <70		–4.1	–32.2	F/M††
ED7-R4	Wadi Abu Safera	23.0265	35.5825	Productive well (S†)			–4.4	–36.3	F/M††
ED7-R-12	Wadi El Nakheil	26.1478	34.1146	Open well (S†)		28.7	–4.9	–36.9	F/M††
ED7-R-19	Wadi Esl 2	25.9345	34.3486	Open well (Alv§, S†)		12.0	–2.7	–19.3	F/M††
ED04-2-1	Sheikh Shazly	24.2000	34.6352	Open well (FB#)			–2.7	–14.2	M§§
ED04-2-2	Bir Um Ghanam	24.7680	34.5170	Open well (FB#)			–2.0	–1.9	M§§
ED04-2-3	Bir Hafafi	24.7240	34.5620	Open well (FB#)			–1.3	–5.7	M§§
ED04-2-4	Bir Fawakhir	26.0120	33.6000	Open well (FB#)			–1.9	–8.3	M§§
ED5A-2	Bir Barramya East	25.0729	33.7976	Hand-dug well (FB#)	42.7		–1.1	–13.7	M§§
ED6-MS-2	Bir Igla	25.1179	34.7629	Open pit (FB#)	7.8		–1.9	–12.6	M§§
ED6-MS-6	Birr Wadi El Gemal	24.5106	34.7133	Open well (FB#)	12		–2.2	–12.5	M§§
ED04-2-5	Bir Laqita	25.8950	33.1400	Productive well (NSS**)			–7.9	–59.2	F##
ED5A-3	Bir Abbad	25.0267	33.0521	Productive well (NSS**)	3		–7.9	–60.7	F##
ED5A-4	Wadi Noqrah	24.4640	33.3287	Well (NSS**)	<50		–7.7	–58.8	F##
ED05-5	Gamheit 1	23.3862	34.8356	Open pit (NSS**)	3.5	29.6	–9.2	–69.5	F##
ED05-8	Wadi Shait	24.5482	33.1655	Productive well (NSS**)		38.0	–9.5	–73.1	F##
ED05-9	Steel factory well	23.8583	33.2591	Productive well (NSS**)	3.3		–8.1	–64.0	F##
ED05-3	Eiqat 1	23.4964	34.9808	Open well (FB#)	10.6	33.4	0.6	4.5	M/EV***
ED5A-1	Bir Bisah	25.0636	33.9127	Hand-dug well (FB#)	11		3.6	9.4	M/EV***

*Limestone.
†Subsided blocks.
§Alluvial sediments.
#Fractured basement.
**Nubian Sandstone.
††Mixed fossil and modern meteoric groundwater.
§§Modern meteoric groundwater.
##Fossil groundwater.
***Evaporated modern meteoric groundwater.
Note: DWT—depth to water table.

for extensional faults bounding subsided successions within the basement complex (e.g., Wadi Ambagi and Wadi Esl) and for extensional faults bounding the Red Sea scarp in the Gona area and surroundings (Figs. 1 and 3).

Integrated Methodologies: A Regional Perspective

On regional Bouguer gravity anomaly maps (Pohlmann and Deetz, 1987), thick subsided sedimentary successions are represented by negative Bouguer anomalies. Figure 4 shows color-coded contoured Bouguer gravity anomaly data superimposed on color-coded digital elevation data (National Aeronautics and Space Administration Shuttle Radar Topography Mission [SRTM]: 90-m resolution). The spatial distribution of the negative anomalies (areas labeled "a," "b," and "c" on Fig. 4) correlates with that of topographically low areas, specifically with areas subtended between the basement outcrops of the Red Sea Hills (west) and the uplifted basement complex ridge of Esh El Malaha (east) and with the low areas to the east of the ridge. Using the half-width formula procedures (Grant and West, 1965; Telford et al., 1990), the depth to the basement was estimated at 850 m, 2340 m, and 925 m for areas labeled "a," "b," and "c," respectively, on Figure 4. Given the coarse resolution (scale: 1:500,000) of the available gravity data, and the complexities of the structures along the rift, not all subsided successions may give rise to negative anomalies on the large-scale Bouguer gravity anomaly maps described above.

We used observations extracted from Landsat TM ratio maps such as the ones displayed in Figure 2A and false-color TM bands (2, 4, and 7), as well as geologic maps (Klitzsch et al., 1987a, 1987b, 1987c, 1987d, 1987e, 1987f), to map the distribution of the subsided blocks within the basement complex and along the coastal plains. We targeted thick layered pre-rift and synrift sedimentary successions that are juxtaposed against, and separated by, faults from older Neoproterozoic basement terrains. Specifically, we targeted the pre-rift Cretaceous Nubian Sandstone in the Duwi area and the upper Oligocene to lower Miocene Nakheil Formation sandstone, the two most productive formations in the coastal Red Sea areas. Two types of deposits were reported for the Nakheil Formation: coarse breccia and fine-grained lacustrine deposits with a thickness of up to 60 m (Akaad and Dardir, 1966). The Nubian Sandstone is represented by thick, nonmarine cross-bedded sandstone and conglomerate (regressive phase) alternating with bedded mudstone and fine-grained sandstone (transgressive phase). Although the thickness of the Nakheil Formation is typically less than that reported for the Nubian, targeting this formation for groundwater exploration is appealing for a number of reasons: (1) the aquifer is shallow compared to the Nubian Sandstone; and (2) it could potentially be recharged by groundwater ascending via the subvertical rift-related faults from the underlying Nubian aquifer or from recharge areas where the Nakheil Formation crops out. Rift-related aquifers are not restricted to sandstone formations—the aquifer properties (porosity and permeability) of the extensive pre-rift limestone units (e.g., Duwi Formation) may be enhanced locally by fracturing and faulting associated with the extension process.

Favorable field relations for aquifer development include extensive outcrops to facilitate groundwater recharge and large aquifer thickness to host and transmit the infiltrating groundwater. In the Duwi area, the Nubian Sandstone (Taref Formation) covers 39 km^2 in outcrop. Knowing the average dip (21° NE) of this formation, we estimate formation thickness ranging from 200 to 400 m that could potentially host an approximate volume of 3.8×10^9 m^3 of groundwater under saturated conditions using

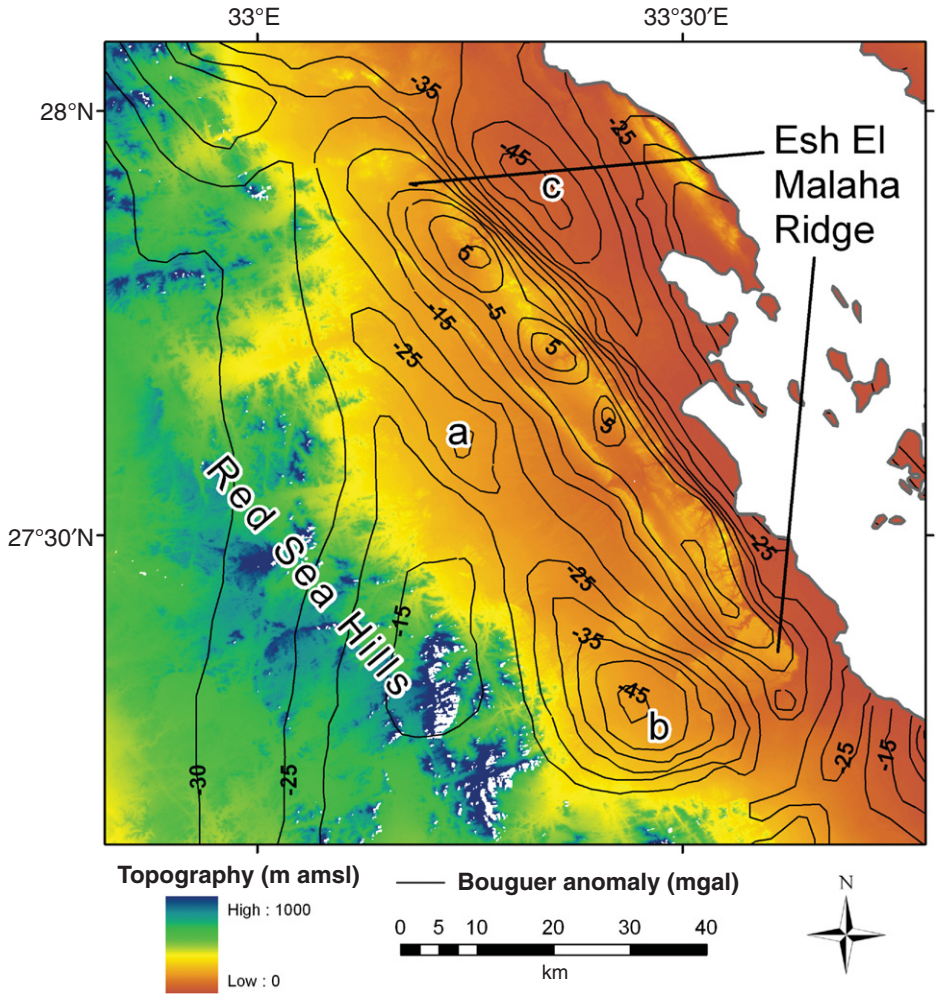

Figure 4. Bouguer gravity anomaly map for the Esh El Malaha area and surroundings. The negative anomalies (marked "a," "b," and "c") are interpreted to indicate thick subsided sedimentary successions.

an average porosity of 25%. Reported porosities for the Nubian aquifer range from 25% to 30% (Evans et al., 1991). The Nakheil Formation in the Duwi area covers an area of 23 km^2 with thicknesses ranging from 70 to 400 m. Assuming an average porosity of 25%, this formation could potentially host an approximate volume of 1.8×10^9 m^3 of groundwater. Subsided pre-Miocene sedimentary successions within the basement complex were observed; a total of nine rift-related subsided pre-Miocene groundwater aquifers were identified (B1 through B9 on Fig. 3). First-order estimates of groundwater volumes in these subsided blocks collectively (excluding those in the Duwi area) were estimated at 1.1×10^9 m^3 and 5.9×10^9 m^3 for the Nakheil Formation and Nubian Sandstone Group, respectively.

Within the coastal plains of the Red Sea and Gulf of Suez, it is sometimes difficult to ascertain the thickness and the composition (sedimentary versus crystalline basement) of the subsided successions, which are now largely covered and obscured by overlying thick alluvial deposits. The presence of scattered basement outcrops within the coastal plain is interpreted to indicate shallow basement and absence of preserved thick sedimentary successions (e.g., areas labeled "a"; Fig. 3). The presence of scattered, tilted pre-Miocene outcrops, however, is interpreted as an indication of the presence of potential rift-related groundwater aquifers at depth. Examples of such areas are at the intersection of Wadis Queih, Hamra, Al Nakheil, Ambagi, Sharm Al Qibli, and Sharm Al Bahri with the coastal plain. Satellite data products and published geologic maps were analyzed in a GIS environment to map the distribution of these scattered pre-Miocene outcrops and to infer their composition and age.

Integrated Methodologies: A Local Perspective

Conventional Electrical Resistivity (ER)

Conventional Electrical Resistivity (ER) investigations were conducted to investigate whether groundwater accumulations are to be found within the target rift-related aquifers that were selected using geological observations and remote sensing and regional gravity data sets, i.e., the ones within the crystalline basement and the others flooring the Red Sea coastal plain. We used vertical electrical soundings (VES) with expanding electrode spacings (Schlumberger array) or horizontal profiling along transects using a constant electrode spacing. Cross sections were generated for each of the investigated sites from the estimated apparent resistivity (ρ) and thickness (h) values for the different VES locations, using the Grapher™, Surfer™, and Rockware™ software. The Resist™ 1987 and Resix™ 1996 software were used for quantitative inversion of the geoelectrical sounding (VES) curves and estimation of ρ and h values. The geoelectric layers were interpreted as geologic layers or lithologies by correlation with field observations (e.g., geologic cross sections), well log or borehole data (Wadi Al Nakheil), and parametric measurements (Wadi Queih). One of the reported sections (Wadi Al Nakheil) was measured and the other cross section (Wadi Queih) was reprocessed, reanalyzed, and reinterpreted from previous work (Mahmoud, 2001). Resistivity equipment used for the collection of our data and for the collection of the reanalyzed published data was the ABEM Terrameter models SAS1000 and SAS4000.

A NW-SE–trending cross section (subparallel to the general strike of beds) was generated along Wadi Al Nakheil from five vertical electrical soundings (V1 through V5; Table 1, Fig. 5A). Five geoelectric units were detected and interpreted as the following geologic units (from bottom to top): (1) Thebes limestone Formation (ρ: 60–310 ohm-m) with undetected thicknesses, (2) water-bearing Nakheil sandstone (ρ: 60–130 ohm-m; thickness: 112–144 m), and (3) undivided zone of Um Mahra and Abu Dabab formations that is formed of intercalations of sandy clay, siltstone, and claystone (ρ: 5–16 ohm-m; thickness: 32 m to 109 m). The pre-rift sequences (units 1, 2, and 3) are overlain by a sandy clay layer (ρ: 30–70 ohm-m; thickness: 32–39 m) that is interpreted to be part of the Issawiya Formation, and wadi fill (ρ: 140–803 ohm-m; thickness: 19–32 m).

A WNW-ESE–trending cross section at right angles with the general strike of beds was generated along Wadi Queih from five vertical electrical soundings (V1 through V5; Table 1 and

TABLE 1. CONVENTIONAL ELECTRICAL RESISTIVITY DATA FOR WADI AL NAKHEIL AND WADI QUEIH

Location	Water-bearing unit	Calibration method	VES* (no.)	DTW† (m)	Thickness (m)
Wadi Al Nakheil	Nakheil Formation	1—Well data	V1		
		2—Field observations	V2	36	89
		3—Geologic section	V3	45.6	96
			V4	168	110
Wadi Queih	Fractured limestone	1—Parametric measurements	V1		
	Duwi Formation	2—Field observations	V2	12.4	54
		3—Geologic section	V3	14	56
	Nubian Sandstone		V4	15.5	62
			V5		

*VES—vertical electrical sounding.
†DTW—depth to water table.

Fig. 5B). Five geoelectric units were detected in addition to the underlying basement complex (fractured and crystalline) and interpreted as the following geologic units from bottom upwards: (1) Nubian Sandstone Group (ρ: 135–137 ohm-m) with undetected thicknesses, (2) Quseir Formation (ρ: 7–10 ohm-m; thickness: 37–43 m), and (3) Duwi Formation which is a saturated fractured limestone aquifer (ρ: 81–95 ohm-m; thickness: 50–59 m). The pre-rift sequences (units 1, 2, and 3) are overlain by a surface layer that is interpreted as wadi deposits (ρ: 140–630 ohm-m; thickness: 5–22 m). These units rest on fresh basement units (ρ: ~15,730 ohm-m) or fractured and/or weathered basement (ρ: ~2550 ohm-m) rock units. Although not shown, similar cross sections were generated for the two remaining locations (Wadi Ambagi and Wadi Hamra; Fig. 3). In Wadi Ambagi the saturated unit is the Nakheil sandstone (16–240 m), and in Wadi Hamra it is fractured limestone of the Duwi Formation (30–86 m).

Very Low Frequency

Very low frequency (VLF) methods (Paterson and Ronka, 1971) were used to test whether extensional faults associated with Red Sea rifting could have acted as conduits allowing groundwater from deeper aquifers to mix with overlying shallower aquifers in subsided blocks, or to discharge at the surface as springs or at near-surface levels in alluvial aquifers flooring the valleys. The VLF is ideal for detecting conductive water-saturated, subvertical breccia zones in bedrock (Palacky et al., 1981), and thus it could be useful in detecting extensional faults that are saturated with ascending groundwater. Because the instrument's detection is limited to within an ~90° fan of strikes (±45° from the radial azimuth to the transmitting station), measurements were made along transects using transmitting stations (e.g., France and Russia; Cutler, Maine (U.S.) and Germany), separated by as large an azimuth as possible. All measurements were acquired during daylight hours, a time when the overhead ionosphere is well developed (Vallée et al., 1992). To avoid interference resulting from sudden pulsation of solar winds that manifest themselves as a sudden decrease or increase in the percent tilt, followed by a gradual recovery over several minutes, averaging or stacking of readings at a given location had to be suspended and restarted after such transients were observed.

Four sites were visited over a period of six days, and a total of seven VLF transects were surveyed in the horizontal profiling mode along transects ranging from 160 m to 1200 m, with station spacing of 10, 20, or 25 m. Usable VLF transmitting stations were almost all in the NW quadrant, with Rugby, England (19.6 kHz), France (20.9 and 21.75 kHz), and Germany (23.4 kHz) providing the strongest signals. Attempts to use a more northerly station (Moscow, 17.1 kHz) resulted in very weak signals. Signals from a more westerly azimuth (Cutler, Maine, 24 kHz) were used for several days. In general the data set with the stronger signal was used for making the final plots. The VLF data of this study were first smoothed with a 3-point running average filter, then transformed using the Fraser filter (Fraser, 1969) that provides readily interpretable plots. Using this filter, dip angle or percent tilt of the field departure from horizontal are plotted along the traverse, and a conductive subsurface anomaly is represented as a peak.

Very low frequency profiles were conducted along transects in Wadi Esl (VLF 14-1 through VLF 14-4) and Wadi Ambagi (VLF 15-1) (Fig. 6). Wadi Esl and Wadi Ambagi are E-W– to NE-SW–trending wadis that crosscut the basement complex and subsided blocks of pre- and synrift sequences, and ultimately drain toward the Red Sea coastal plain. The wadis intersect extensional faults bounding the subsided blocks within the basement complex proximal to the coastal plain. Both areas have one or more horsts surrounded by downdropped blocks (half-graben) that subsided along N-S– to NW-trending faults that were observed in the field. For both wadis, VLF anomalies were observed along the postulated extension of these faults in the main valley. The most pronounced anomalies in Wadi Esl were identified along two VLF traverses (VLF 14-2 and VLF 14-4), where tilts of up to 40% were observed. The VLF observations together with our field relations and those extracted from geologic maps (e.g., Klitzsch et al., 1987a, 1987f) were used to generate interpretation maps showing the inferred distribution of significant extensional faults in Wadi Esl and Wadi Ambagi (Fig. 7). No vegetation was observed along the first 950 m of the Wadi Ambagi line, whereas the last 250 m had abundant shrubs and sedges indicating shallow water, as the Precambrian rocks and the fault plane(s) bounding the basement approached the surface. The productive well in Wadi Esl and the spring in Wadi Ambagi are located along the postulated extension of N-S– to NW-trending extensional faults observed in the field, supporting the VLF-based suggestion that groundwater is ascending along these faults.

Additional VLF profiles were conducted at two other locations, Gona North-1 (VLF 16-1), and Gona North-2 (VLF 16-2) (Fig. 6), along E-W–trending wadis crosscutting extensional faults that separate the Gulf of Suez scarp from the coastal plain (Klitzsch et al., 1987b, 1987f). In both sites, the scarps are defined by NW-trending fault systems with upthrows inland and downthrows toward the Gulf of Suez. The VLF investigations were conducted to examine whether groundwater from deep pre-rift aquifers (e.g., Nubian aquifer) within subsided blocks ascends along these extensional faults feeding the overlying alluvial aquifers.

The starting point for Profile VLF 16-1 in Gona North-1 is in the steep-walled canyon that cuts Precambrian rocks, and extends out onto the head of the alluvial fan. The profile crosses a series of normal faults, down to the east, that strike parallel to the mountain front and to the Red Sea–Gulf of Suez coast. A large anomaly (tilt: >30%; Fig. 6) was observed at the mouth of the canyon above the postulated extension of the main fault into the wadi where the VLF measurements were made. In this area, the examined fault defines the scarp. The Gona North-2 location is similar to the preceding location in its geologic and hydrologic setting. Again, one VLF traverse was conducted along an E-W–trending wadi intersecting the NW-trending fault system that controls a major NW-trending cliff bounding the coastal plain. The VLF tilt anomalies (16.7%) were observed along the traverse and are interpreted as indicating the locations of ascending groundwater along deep fault systems. In summary, we interpret the observed spatial correlation of the VLF anomalies with the location of major NW- or N-S–trending faults in the four examined

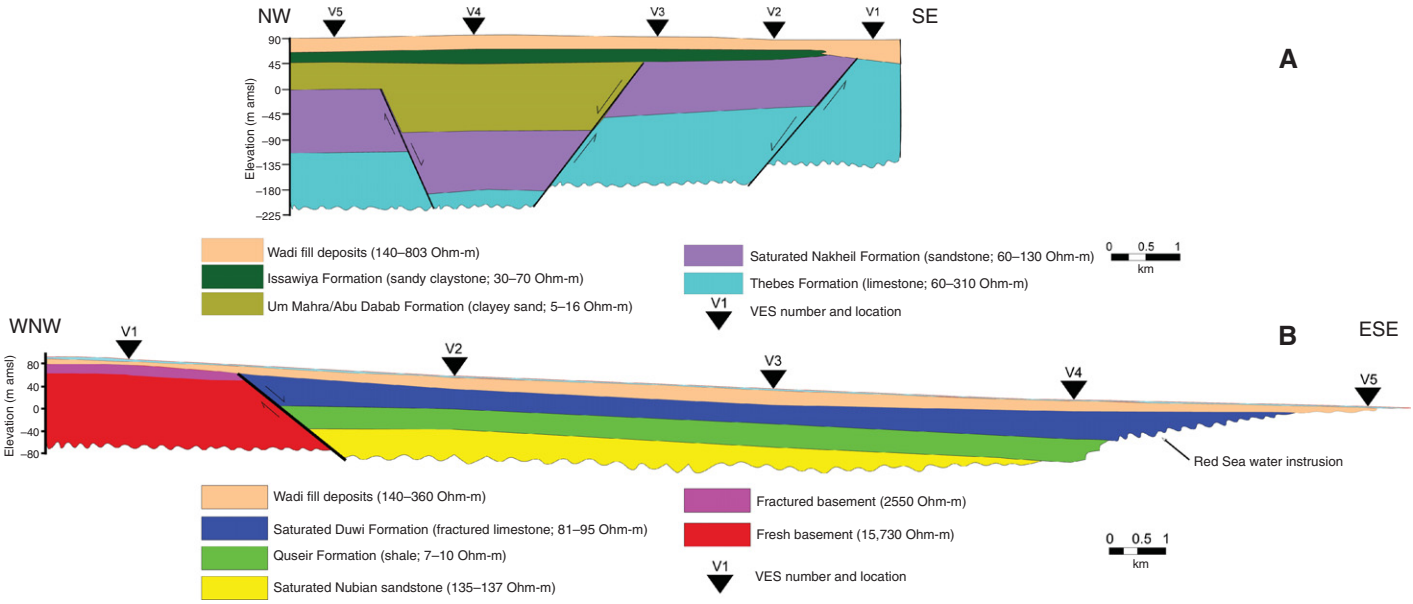

Figure 5. Geoelectric cross sections: (A) NW-SE–trending cross section subparallel to the general strike of beds, generated along Wadi Al Nakheil from five vertical electrical soundings. (B) WNW-ESE–trending cross section, generated along Wadi Queih from five vertical electrical soundings. Vertical to horizontal exaggeration factor is 10 for each of cross sections "a" and "b."

locations as indicative of groundwater ascent along major normal faults that were propagated or reactivated at the onset of the Red Sea rifting.

Hydrogen and Oxygen Stable Isotope Data

Insights into the origin of the groundwater, the timing of its recharge, and mechanisms of discharge were gained from the analysis of their isotopic composition. Twenty-four groundwater samples were collected for isotopic analyses of H and O within H_2O as shown in Table 2 and Figure 8. Groundwater samples were collected from the locations identified as subsided blocks along the Gulf of Suez and the Red Sea coastal plains (ED3-15, ED3-16, ED3-17, and ED5A-8) and from the subsided blocks within the basement complex in proximity to the coastline (ED6-MS1, ED6-MS7, ED7-R4, and ED7-R12) (Fig. 1 and Table 2). Additional samples were collected from fractured basement and overlying alluvial sediments (ED-04-2-1, ED-04-2-2, ED-04-2-3, ED-04-2-4, ED5A-2, ED6-MS-2, and ED6-MS-6) and from the artesian and production wells tapping the Nubian Sandstone aquifer at depth (ED04-2-5, ED5A-3, ED5A-4, ED05-5, ED05-8, and ED05-9).

Groundwater samples were collected in high-density polyethylene bottles and tightly capped. Stable isotope ratios of H and O in water were measured at Isotech Laboratories in Champaign, Illinois. Hydrogen isotope ratios were measured by the Zn reaction method (Kendall and Coplen, 1985), using a Finnigan Delta Plus XL isotope-ratio mass spectrometer (IRMS). Oxygen isotope ratios were measured by the CO_2 equilibration method (Nelson, 2000), using a Finnigan Delta S IRMS. Hydrogen and O isotope data are reported in terms of the conventional delta (δ) notation, in units of permil deviation relative to a standard reference, whereby

$$\delta\ (‰) = [(R_{sample}/R_{standard}) - 1] \times 10^3$$

and R = $^2H/^1H$ or $^{18}O/^{16}O$, and the standard is Vienna standard mean ocean water (Coplen, 1996). Precisions of δD and $\delta^{18}O$ values are ±2 and ±0.1‰, respectively.

Additional insights into the origin of the groundwater from the subsided blocks were made through comparisons to fossil and modern groundwater data from the Western Desert, Eastern Desert, Sinai, and modern precipitation data. Figure 8 includes data for samples from the present study as well as: (1) fossil groundwater from the Nubian aquifer of the Western Desert of Egypt (Sultan et al., 1997; Patterson et al., 2005); (2) fossil groundwater from the Nubian aquifer of the Sinai Peninsula (Sturchio et al., 1996); (3) modern meteoric groundwater from the shallow alluvial aquifers in Wadi Tafra, a major E-W–trending valley (Fig. 1) that originates from the Red Sea Hills and drains into the Nile River (Sultan et al., 2000); and (4) data for modern precipitation from Sidi Barrani and the Negev desert (IAEA and WMO, 1998).

Water within the subsided blocks had low δD and $\delta^{18}O$ values (δD: –19.3‰ to –53.9‰; $\delta^{18}O$: –2.7‰ to –7.1‰) compared to groundwater samples in fractured basement rocks and the overlying alluvial aquifers (e.g., Sheikh El Shazly, Bir Um Ghanam, Bir Hafafit, Bir Fawakhir, Bir Barramya East, Bir Igla, and Bir Wadi El Gemal). The samples from the fractured basement and the overlying alluvial aquifers have isotopic compositions (δD: –1.9‰ to –14.2‰; $\delta^{18}O$: –1.1‰ to –2.7‰) similar to those of modern precipitation (δD: –3.0‰ to –26.0‰; $\delta^{18}O$: –2.0‰ to –6.0‰) or evaporated modern precipitation sampled in the Wadi Tarfa area (Sultan et al., 2000) (Fig. 8 and Table 2). The groundwater samples of the Wadi Tarfa area are mostly evaporated meteoric waters, with relatively short underground residence times indicated by the presence of live tritium (i.e., <45 yr) (Sultan et al., 2000). The groundwater in fractured basement and in the overlying alluvial aquifers is here interpreted to have a modern meteoric origin.

The samples from the subsided blocks have higher δD and $\delta^{18}O$ values compared to those of the Western Desert fossil groundwater and display a wider range in their isotopic compositions (Table 2). The isotopic compositions of the groundwater from subsided blocks could be accounted for as mixtures of two end members: (1) fossil Nubian aquifer groundwater having more depleted compositions similar to those of the Western Desert Nubian Sandstone aquifer, and (2) precipitation having more enriched compositions similar to those reported for modern precipitation from Sidi Barani and Negev deserts (Fig. 8 and Table 2). The depleted isotopic

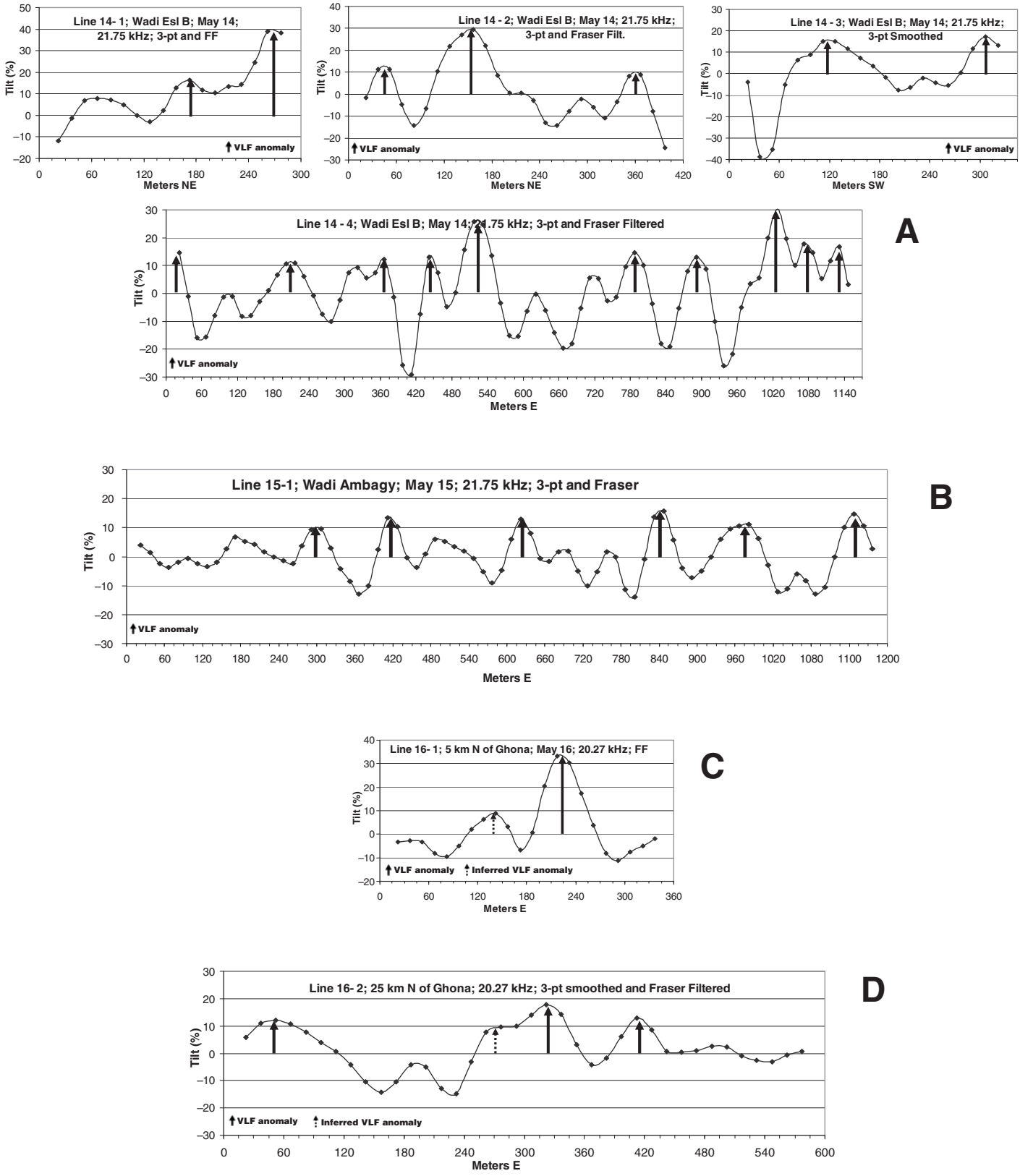

Figure 6. Locating conductive extensional faults in Wadi Esl, Wadi Ambagi, Gona North-1, and Gona North-2 using very low frequency (VLF) data. (A) The VLF transects 14-1, 14-2, 14-3, and 14-4 in Wadi Esl. (B) VLF transects 15-1 in Wadi Ambagi. (C) VLF transect 16-1 in Gona North-1. (D) VLF transect 16-2 in Gona North-2. The pronounced tilt anomalies (solid arrows) mark the locations of the conductive water-saturated, subvertical faults. Faults inferred from weaker anomalies (dashed arrows) are suspect. FF—Fraser filtered.

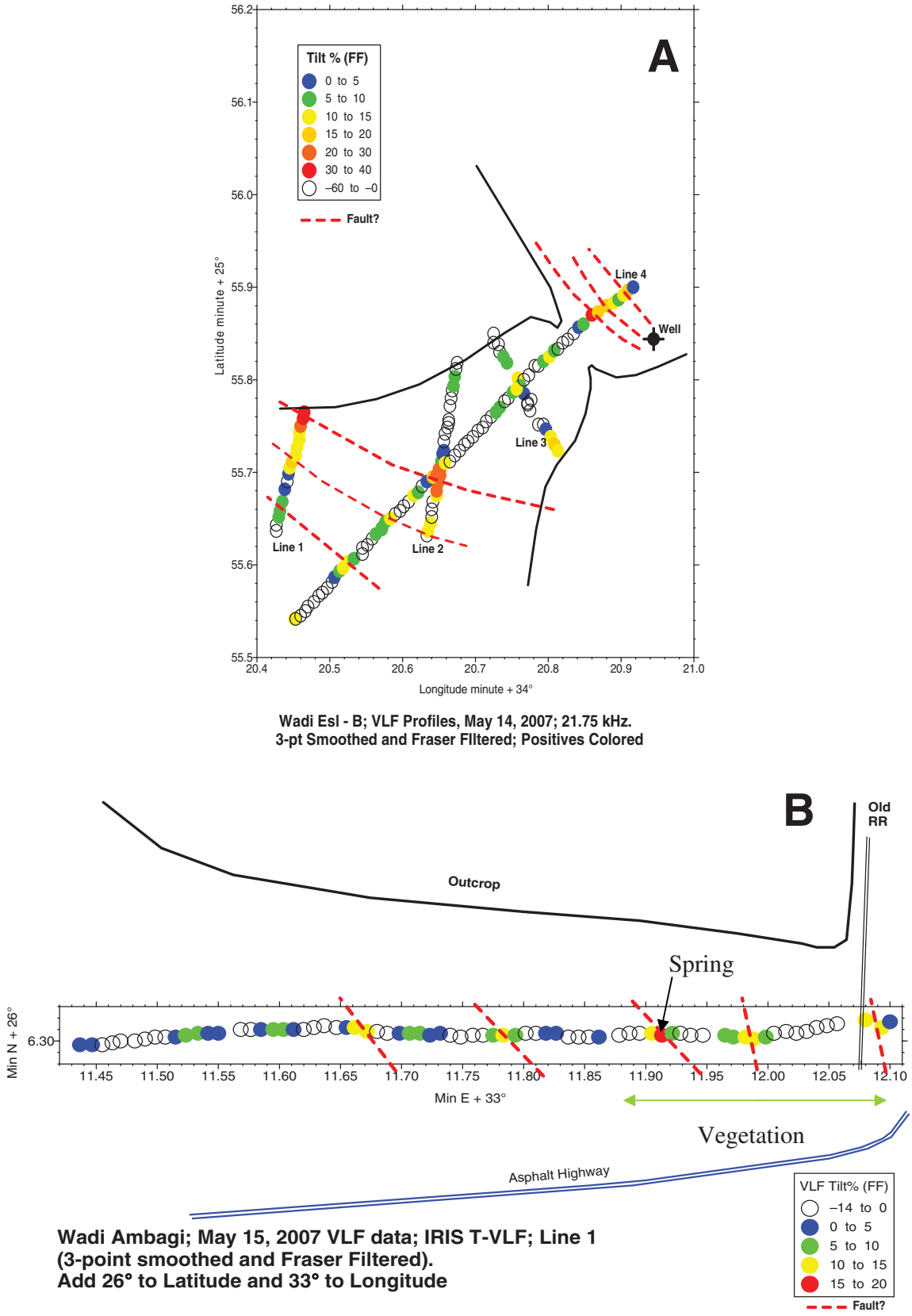

Figure 7. Sketch interpretation maps showing the distribution of inferred extensional faults based on very low frequency (VLF) data and field relations. (A) Sketch map for Wadi Esl. (B) Sketch map for Wadi Ambagi. Also shown are well and spring locations in Wadi Esl and Wadi Ambagi, respectively. FF—Fraser filtered; RR—Railroad.

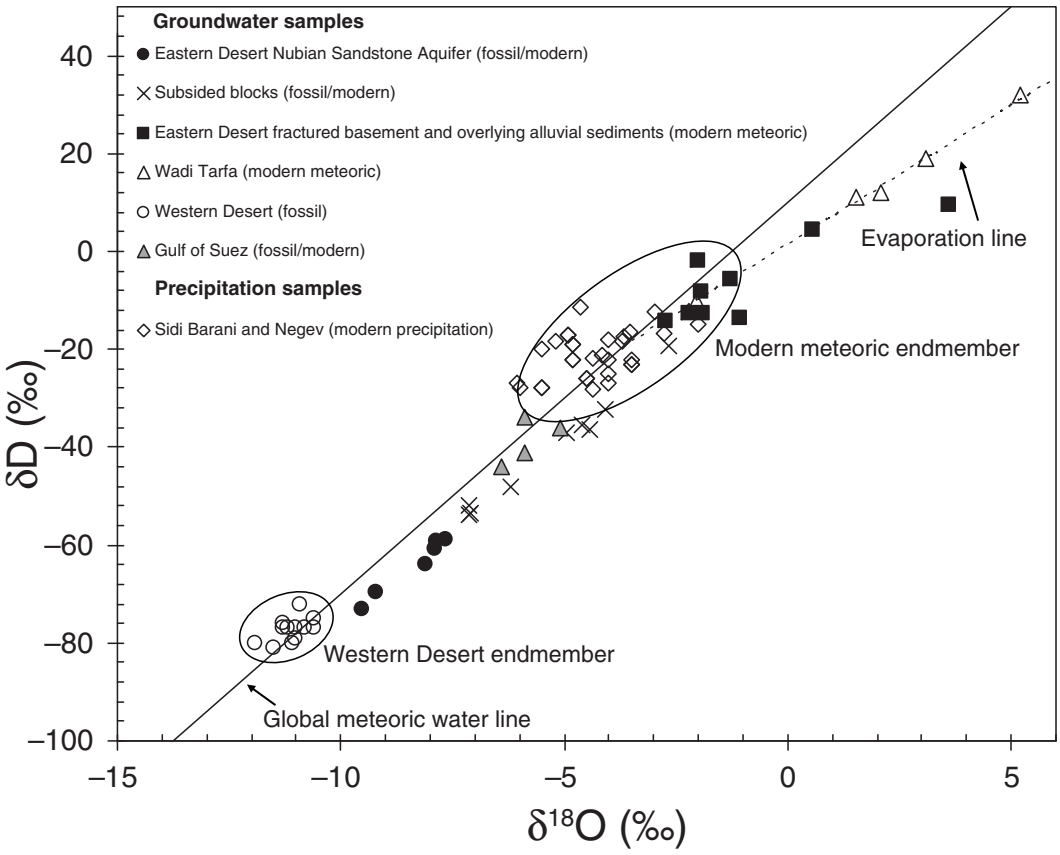

Figure 8. Comparison between stable isotope values [hydrogen (δD) versus oxygen ($\delta^{18}O$)] for groundwater samples from the Eastern Desert subsided blocks with: (1) shallow aquifers in fractured basement and overlying alluvial sediments; and (2) artesian and production wells tapping the Nubian Sandstone aquifer at depth. Also shown are: (1) modern meteoric groundwater from the Wadi Tarfa area (Sultan et al., 2000); (2) fossil groundwater from the Western Desert (Sultan et al., 1997; Patterson et al., 2005) and from the Sinai Peninsula (Sturchio et al., 1996); and (3) modern precipitation from Sidi Barrani and Negev (IAEA and WMO, 1998). Solid line—global meteoric water line, $\delta D = \delta^{18}O + 10$ (Craig, 1961); dotted line—evaporation line for the Wadi Tarfa groundwater samples (Sultan et al., 2000).

composition of the Western Desert Nubian aquifer fossil water is best explained by recharge of precipitation showing the "continental effect" (Dansgaard, 1964), i.e., progressive condensation of water vapor from paleowesterly wet oceanic air masses that traveled across North Africa, during wet climatic periods at least as far back as 450,000 yr before the present (Sonntag et al., 1978; Sultan et al., 1997; Sturchio et al., 2004). Assuming simple mixing between two end members, one with compositions similar to those of the Western Desert fossil groundwater and another with compositions similar to those of modern precipitation, we estimate that the recharge during previous wet climatic periods contributed 35%–70% by volume of the groundwater in the subsided blocks (Fig. 8).

The groundwater samples from the subsided blocks of the Eastern Desert have intermediate isotopic compositions between the Western Desert fossil groundwater and the Sinai fossil groundwater, possibly reflecting a geographic trend in the isotopic composition of paleoprecipitation recharge into the Nubian aquifer. Examination of patterns of modern precipitation suggests an alternative explanation. Currently, rainfall amounts over the Nubian Sandstone outcrops (recharge areas) in southern Sinai are considerable (~100 mm/yr) compared to that in the Western Desert, which hardly receives any precipitation (0–5 mm/yr) (EMA, 1996; Legates and Wilmott, 1997; Nicholson, 1997). Precipitation amounts in the Eastern Desert are intermediate between that reported for the Western Desert and that for Sinai. Thus, the apparent progressive enrichment in the isotopic composition from west (Western Desert; δD: ~–80‰, $\delta^{18}O$: ~–12‰) to east (Sinai: δD: ~–40‰, $\delta^{18}O$: ~–4‰) could reflect variable degrees of mixing between fossil water that recharged during wet climatic periods and meteoric waters that were recharged during the intervening dry climatic periods such as those experienced at present conditions. Regardless of which hypothesis is adopted, groundwater samples from the subsided blocks that have depleted isotopic compositions must have been derived at least in part from the fossil water because their anomalously low δD and $\delta^{18}O$ values cannot be explained by recharge of modern precipitation.

These depleted isotopic compositions were used as additional criteria for identifying rift-related aquifers, and were especially valuable to infer the presence at depth of these aquifers in areas where no outcrops of pre-rift sequences were observed or reported and where no detailed geophysical data are available. Examples of such samples, areas, and inferences were made in the Wadi Ambagi area (ED6-MS-1) and Wadi Abu Safera (ED7-R4) (Fig. 1 and Table 2). The isotopic data are also used to support our earlier findings from VLF investigations, which indicated that extensional faults could have acted as conduits for groundwater ascending from subsided blocks (Sultan et al., 2008b). The observed similarities in isotopic compositions of groundwater from subsided blocks and springs from the same area are consistent with this suggestion. The isotopic composition of groundwater from a well (ED7-R-12) tapping subsided Nakheil formation in Wadi Al Nakheil is similar to that of groundwater discharging in Wadi Ambagi spring (ED6-MS-1), only a few kilometers away (δD: ED7-R-12: –36.9‰; ED6-MS-1: –35.4‰) (Table 2). Similar observations were made in the Wadi Darah area. The isotopic composition of groundwater (sample ED 3-17) from a production well tapping the Nubian Sandstone and groundwater (sample ED 3-15) from an open pit are similar (δD: ED 3-17: –52.0‰; ED 3-17: –53.9‰).

DISCUSSION AND SUMMARY

Using the Red Sea rift as an example, this study highlights the important role of rifting environments in providing settings conducive

for groundwater aquifer development. Like all rifts, the Red Sea opening was associated with uplift and extension; the uplift of the crystalline rock and the overlying thick sedimentary successions exposed the sequence to extensive erosion. The extension provided opportunities for the preservation of the stratigraphic sequences as subsided blocks within the basement complex, proximal to or underlying the coastal plain and/or the Gulf of Suez and the Red Sea. Currently, all the highly productive wells in the Eastern Desert are tapping subsided blocks to the east and west of the Red Sea Hills. Examples include the Upper Jurassic–Upper Cretaceous sandstone aquifers (Taref Formation of the Nubian Sandstone Group) and upper Oligocene to lower Miocene sandstone (Nakheil Formation). We also speculate that the aquifer properties (porosity and permeability) of the extensive, more massive pre-rift units (e.g., Duwi limestone aquifers) are enhanced by fracturing and faulting associated with the extension process.

An integrated (field, geochemical, geophysical, and remote sensing–GIS) approach was adopted to demonstrate ways by which Red Sea rift–related subsided groundwater aquifers could be identified and verified. The distribution of potential aquifers in thick subsided blocks was achieved by the analysis of regional gravity data, where these thick subsided sedimentary successions are represented by negative Bouguer anomalies. Observations extracted from geologic maps and satellite data, processed in ways to emphasize lithologic and structural variations, were used to identify the distribution of the relatively small groundwater aquifers. Verification of these inferences was enabled using geophysical (e.g., VES) data to determine the depth to, and thickness of, the saturated zones. Structural definition of the deeper basins that are beyond the reach of the VES method will require detailed gravity surveying.

We suggest that the extensional faults associated with the Red Sea rifting could have acted as conduits for ascending groundwater from the subsided aquifers as evidenced by: (1) discharge of fossil groundwater from hot springs along the Red Sea coastal plain (Sturchio et al., 1996), and (2) VLF investigations indicating that the examined subvertical extensional faults proximal to the coastal plain are water-bearing conductive discontinuities. The extensional faults also could have facilitated the mixing of ascending Nubian aquifer groundwater with groundwater in overlying aquifers over time (Sultan et al., 2007). The observed similarities in isotopic compositions of groundwater from subsided blocks and springs from the same area are consistent with this suggestion.

The stable isotopic compositions of groundwaters from these subsided blocks set them apart from other aquifers recharged by modern precipitation, an observation that was used to further validate their distribution. Comparisons of the isotopic compositions of groundwater samples from the various subsided blocks indicate that they are generally more depleted than Eastern Desert aquifers (e.g., fractured basement), that are fed by modern precipitation, but less depleted than the fossil water of the Western Desert aquifers, suggesting that they are probably mixtures of modern and fossil waters. We suggest that the opening of the Red Sea and the Gulf of Suez provided opportunities for the preservation of the stratigraphic sequences including the Nubian Sandstone Group and the Nakheil Formation within the subsided blocks. As described earlier, some of these blocks were tilted in the process of the Red Sea opening, providing opportunities for aquifer recharge where the aquifer units within the tilted blocks crop out. The isotopic compositions of groundwater from these aquifers are best interpreted as indicating aquifer recharge in previous wet climatic periods with modest contributions during intervening dry periods similar to those present conditions.

Results indicate that the groundwater potential for the investigated aquifers is high with estimates for groundwater volumes of up to 3×10^9 m^3 and 10×10^9 m^3 for subsided blocks of the Nakheil and Taref formations, respectively, within the basement complex of the Central Eastern Desert alone (excluding coastal plain aquifers). This study highlights the potential for identifying similar rift-related aquifer systems along the length of the Red Sea–Gulf of Suez system, and in rift systems elsewhere. One of the significant features of these Red Sea–related aquifers is that they are receiving modern precipitation. Additional studies are needed to quantify these modern contributions for each of the identified aquifers to assist in the development of sustainable extraction scenarios. Water quality investigations are also necessary prior to aquifer development because it has been shown that the Nubian Sandstone in neighboring Jordan could contain high levels of natural radioactivity (Vengosh et al., 2009). Such investigations and studies could ultimately contribute to addressing water scarcity problems in the region.

ACKNOWLEDGMENTS

We thank the Editor, the Associate Editor, and the reviewers of the GSA Bulletin for their constructive comments and the administration of Suez Canal University, Cairo University, and the Egyptian Ministry of Water Resources and Irrigation for the logistical support provided. We thank Professor Yehia Abdel Hady for his instrumental role in initiating and facilitating the development of this project. Funding was provided by the United Nations Development Programme; the Global Environmental Facility International Water Program; National Science Foundation science and technology grant OISE-0514307; and the North Atlantic Treaty Organization, Science for Peace Program grant SFP982614 (Environmental Security Program), all awarded to Western Michigan University.

REFERENCES CITED

Abdel-Gawad, M., 1970, The Gulf of Suez—A brief review of stratigraphy and structure: Philosophical Transactions of the Royal Society of London, Series A: Mathematical and Physical Sciences, v. 267, p. 41–48, doi: 10.1098/rsta.1970.0022.

Abuzeid, H.T., 1994, Geology of the Wadi Hamrawin area, Red Sea Hills, Eastern Desert, Egypt [Ph.D. thesis]: Columbia, University of South Carolina, 206 p.

Agar, R.A., 1987, The Najd fault system revisited—A two-way strike-slip orogen in the Saudi Arabian Shield: Journal of Structural Geology, v. 9, p. 41–48, doi: 10.1016/0191-8141(87)90042-3.

Akaad, S.E., and Dardir, A., 1966, Geology of the Red Sea Coast between Ras Shagra and Mersa Alam with short note on exploratory work at Gebel El Rusas lead-zinc deposits: Geological Survey of Egypt Paper 35, 67 p.

AlSharhan, A.S., 2003, Petroleum geology and potential hydrocarbon plays in the Gulf of Suez rift basin, Egypt: American Association of Petroleum Geologists Bulletin, v. 87, p. 143–180.

Bosworth, W., Huchon, P., and McClay, K., 2005, The Red Sea and Gulf of Aden Basins: Journal of African Earth Sciences, v. 43, p. 334–378, doi: 10.1016/j.jafrearsci.2005.07.020.

Brown, G.F., and Coleman, R.G., 1972, The tectonic framework of the Arabian Peninsula: 24th International Geological Congress, v. 3, p. 300–305.

Coplen, T.B., 1996, New guidelines for the reporting of stable hydrogen, carbon, and oxygen isotope ratio data: Geochimica et Cosmochimica Acta, v. 60, p. 3359, doi: 10.1016/0016-7037(96)00263-3.

Craig, H., 1961, Isotopic variations in meteoric waters: Science, v. 133, p. 1702–1703, doi: 10.1126/science.133.3465.1702.

Dansgaard, W., 1964, Stable isotopes in precipitation: Tellus, v. 16, p. 436–468, doi: 10.1111/j.2153-3490.1964.tb00181.x.

Dixon, T.H., Stern, R.J., and Hussein, I.M., 1987, Control of Red Sea rift geometry by Precambrian structures: Tectonics, v. 6, p. 551–571, doi: 10.1029/TC006i005p00551.

Egyptian General Survey Authority (EGSA), 1996a, Abu Sinbil, Sheet NF 36 J: Topographic Sheets, Egyptian Series, EGSA in cooperation with FINNIDA, Finland.

Egyptian General Survey Authority (EGSA), 1996b, Al-Qusayr, Sheet NG 36 K: Topographic Sheets, Egyptian Series, v. 1, scale 1:250,000.

Egyptian General Survey Authority (EGSA), 1996c, Baranis, Sheet NF 36 P: Topographic Sheets, Egyptian Series, v. 1, scale 1:250,000.

Egyptian General Survey Authority (EGSA), 1996d, Jabal Hamatah, Sheet NG 36 D: Topographic Sheets, Egyptian Series, v. 1, scale 1:250,000.

Egyptian General Survey Authority (EGSA), 1996e, Wadi Al-Allaqi, Sheet NF 36 K: Topographic Sheets, Egyptian Series, v. 1, scale 1:250,000.

Egyptian General Survey Authority (EGSA), 1996f, Wadi Al-Barramiyyah, Sheet NG 36 G: Topographic Sheets, Egyptian Series, v. 1, scale 1:250,000.

Egyptian General Survey Authority (EGSA), 1997a, Al-Ghardaqah (Hurghada), Sheet NG 36 O: Topographic Sheets, Egyptian Series, v. 1, scale 1:250,000.

Egyptian General Survey Authority (EGSA), 1997b, Bir Umm Umayyid, Sheet NG 36 N: Topographic Sheets, Egyptian Series, v. 1, scale 1:250,000.

Egyptian General Survey Authority (EGSA), 1997c, Jabal An-Natit, Sheet NF 36 O: Topographic Sheets, Egyptian Series, v. 1, scale 1:250,000.

Egyptian General Survey Authority (EGSA), 1997d, Marsa' Alam, Sheet NG 36 H: Topographic Sheets, Egyptian Series, v. 1, scale 1:250,000.

Egyptian General Survey Authority (EGSA), 1997e, Qina, Sheet NG 36 J: Topographic Sheets, Egyptian Series, v. 1, scale 1:250,000.

Egyptian General Survey Authority (EGSA), 1997f, Wadi Shiayt, Sheet NG 36 C: Topographic Sheets, Egyptian Series, v. 1, scale 1:250,000.

Egyptian Meteorological Authority (EMA), 1996, Climatic Atlas of Egypt: Cairo, Egypt, Egyptian Meteorological Authority, Ministry of Transport and Communications.

Egyptian Ministry of Water Resources and Irrigation (EMWRI), 2004, Well inventory in the Eastern Desert: Internal Report for the United Nations Development Program–funded Eastern Desert Project.

Escartin, J., Hirth, G., and Evans, B., 2001, Strength of slightly serpentinized peridotites: Implications for the tectonics of oceanic lithosphere: Geology, v. 29, p. 1023–1026, doi: 10.1130/0091-7613(2001)029<1023:SOSSPI>2.0.CO;2.

Evans, K., Beavan, J., and Simpson, D., 1991, Estimating aquifer parameters from analysis of forced fluctuations in well level: An example from the Nubian Formation near Aswan, Egypt: 1. Hydrogeological background and large-scale permeability estimates: Journal of Geophysical Research, v. 96, B7, p. 127–137.

Fraser, D.C., 1969, Contouring of VLF-EM data: Geophysics, v. 34, p. 958–967, doi: 10.1190/1.1440065.

Garfunkel, Z., and Bartov, Y., 1977, The tectonics of the Suez rift: Geological Survey of Israel Bulletin, v. 71, 44 p.

Grant, F.S., and West, G.F., 1965, Interpretation Theory in Applied Geophysics: McGraw-Hill, 584 p.

International Atomic Energy Agency (IAEA) and World Meteorological Organization (WMO), 1998, Global Network of Isotopes in Precipitation: The GNIP database, Release 2, May 1998.

Issar, A., 1979, The paleohydrology of southern Israel and its influence on the flushing of the Kurnub and Arad Groups (lower Cretaceous and Jurassic): Amsterdam, Journal of Hydrology, v. 44, p. 289–303, doi: 10.1016/0022-1694(79)90136-7.

Kendall, C., and Coplen, T.B., 1985, Multisample conversion of water to hydrogen by zinc for stable isotope determination: Analytical Chemistry, v. 57, p. 1437–1440, doi: 10.1021/ac00284a058.

Klitzsch, E., List, F.K., and Pohlmann, G., 1987a, Geological map of Egypt, Asyut Sheet: Cairo, Egypt, The Egyptian General Petroleum Corporation and Conoco, scale 1:500,000.

Klitzsch, E., List, F.K., and Pohlmann, G., 1987b, Geological map of Egypt, Beni Suef Sheet: Cairo, Egypt, The Egyptian General Petroleum Corporation and Conoco, scale 1:500,000.

Klitzsch, E., List, F.K., and Pohlmann, G., 1987c, Geological map of Egypt, Bernice Sheet: Cairo, Egypt, The Egyptian General Petroleum Corporation and Conoco, scale 1:500,000.

Klitzsch, E., List, F.K., and Pohlmann, G., 1987d, Geological map of Egypt, Gebel Hamata Sheet: Cairo, Egypt, The Egyptian General Petroleum Corporation and Conoco, scale 1:500,000.

Klitzsch, E., List, F.K., and Pohlmann, G., 1987e, Geological map of Egypt, Luxor Sheet: Cairo, Egypt, The Egyptian General Petroleum Corporation and Conoco, scale 1:500,000.

Klitzsch, E., List, F.K., and Pohlmann, G., 1987f, Geological map of Egypt, Quseir Sheet: Cairo, Egypt, The Egyptian General Petroleum Corporation and Conoco, scale 1:500,000.

Koeppel, I., 2001, Location services are here now: ArcUser, p. 14–17.

Korme, T., Acocella, V., and Abebe, B., 2004, The role of pre-existing structures in the origin, propagation and architecture of faults in the main Ethiopian rift: Gondwana Research, v. 7, p. 467–479, doi: 10.1016/S1342-937X(05)70798-X.

Legates, D.R., and Wilmott, C.J., 1997, Legates surface and ship observation of precipitation: ftp://daac.gsfc.nasa.gov/hydrology/precip/legates/README.legates_gauge_precip.

Mahmoud, H.H., 2001, Geophysical evaluation of the groundwater resources in selected wadis in the coastal plain in the area between Safaga and El Quseir, Red Sea Coast, Egypt [M.S. thesis]: Cairo, Egypt, Ain Shams University, 166 p.

Moore, J.M., 1979, Tectonics of the Najd transcurrent fault system, Saudi Arabia: Journal of the Geological Society of London, v. 136, p. 441–454, doi: 10.1144/gsjgs.136.4.0441.

Moustafa, A.R., 2002, Controls on the geometry of transfer zones in the Suez rift and northwest Red Sea: Implications for the structural geometry of rift systems: American Association of Petroleum Geologists Bulletin, v. 86, p. 979–1002.

Nelson, S.T., 2000, A simple, practical methodology for routine VSMOW/SLAP normalization of water samples analyzed by continuous flow methods: Rapid Communications in Mass Spectrometry, v. 14, p. 1044–1046, doi: 10.1002/1097-0231(20000630)14:12<1044::AID-RCM987>3.0.CO;2-3.

Nicholson, S., 1997, Nicholson's Africa Precipitation: National Center for Atmospheric Research.

Palacky, G.V., Ritsema, I.L. and De Jong, S.J., 1981, Electromagnetic prospecting for groundwater in Precambrian terrains in the Republic of Upper Volta (Burkina Faso): Geophysical Prospecting, p. 932–955.

Paterson, N., and Ronka, V., 1971, Five years of surveying with very low frequency–electro magnetics method: Geoexploration, v. 9, p. 7–26, doi: 10.1016/0016-7142(71)90085-8.

Patterson, L., Sturchio, N.C., Kennedy, B.M., van Soest, M., Sultan, M., Lu, Z., Lehmann, B., Purtschert, R., El Kaliouby, B., Dawood, Y., and Abdallah, A., 2005, Cosmogenic, radiogenic, and stable isotopic constraints on groundwater residence time in the Nubian aquifer, Western Desert of Egypt: Geochemistry Geophysics Geosystems, v. 6, p. Q01005, doi: 10.1029/2004GC000779.

Pivnik, D.A., Ramzy, M., Steer, B.L., Thorseth, J., El Sisi, Z., Gaafar, I., Garing, J.D., and Tucker, R.S., 2003, Episodic growth of normal faults as recorded by syntectonic sediments, July oil field, Suez rift, Egypt: American Association of Petroleum Geologists Bulletin, v. 87, p. 1015–1030, doi: 10.1306/08220201022.

Pohlmann, G., and Deetz, M., 1987, Egypt, Atlas for groundwater 1:500,000 Bouguer gravity anomaly map: Cairo and Berlin, General Petroleum Company; Berlin, Technische Fachhochschule.

Raleigh, C.B., and Paterson, M.S., 1965, Experimental deformation of serpentinite and its tectonic implications: Journal of Geophysical Research, v. 70, p. 3965–3985, doi: 10.1029/JZ070i016p03965.

Reynolds, M.L., 1979, Geology of the northern Gulf of Suez: Annals of the Geological Society of Egypt, v. 9, p. 322–343.

Sonntag, C., Klitzsch, E., Lohnert, E.P., El Shazley, E.M., Munnich, K.O., Junghans, C.H., Thorweihe, U., Weistrofer, K., and Swailem, F.M., 1978, Paleoclimatic information from deuterium and oxygen-18 in carbon-14-dated north Saharian groundwaters: Isotope Hydrology 1978: Proceedings of an International Symposium on Isotope Hydrology: Vienna, International Atomic Energy Agency, p. 569–580.

Stern, R.J., 1985, The Najd fault system, Saudi Arabia and Egypt—A Late Precambrian rift-related transform system: Tectonics, v. 4, p. 497–511, doi: 10.1029/TC004i005p00497.

Sturchio, N.C., Arehart, G.B., Sultan, M., Sano, Y., AboKamar, Y., and Sayed, M., 1996, Composition and origin of thermal waters in the Gulf of Suez area, Egypt: Applied Geochemistry, v. 11, p. 471–479.

Sturchio, N.C., Du, X., Purtschert, R., Lehmann, B.E., Sultan, M., Patterson, L.J., Lu, Z.T., Muller, P., Bigler, T., Bailey, K., O'Connor, T.P., Young, L., Lorenzo, R., Becker, R., El Alfy, Z., El Kaliouby, B., Dawood, Y., and Abdallah, A.M.A., 2004, One million year old groundwater in the Sahara revealed by krypton-81 and chlorine-36: Geophysical Research Letters, v. 31, p. L05503, doi: 10.1029/2003GL019234.

Sultan, M., Arvidson, R.E., Sturchio, N.C., and Guinness, E.A., 1987, Lithologic mapping in arid regions with Landsat thematic mapper data: Meatiq Dome, Egypt: Geological Society of America Bulletin, v. 99, no. 6, p. 748–762, doi: 10.1130/0016-7606(1987)99<748:LMIARW>2.0.CO;2.

Sultan, M., Arvidson, R.E., Duncan, I.J., Stern, R.J., and El Kaliouby, B., 1988, Extension of the Najd shear system from Saudi Arabia to the Central Eastern Desert of Egypt based on integrated field and Landsat observations: Tectonics, v. 7, p. 1291–1306, doi: 10.1029/TC007i006p01291.

Sultan, M., Becker, R., Arvidson, R.E., Shore, P., Stern, R.J., El Alfy, Z., and Guinness, E.A., 1992, Nature of the Red Sea crust—A controversy revisited: Geology, v. 20, p. 593–596, doi: 10.1130/0091-7613(1992)020<0593:NOTRSC>2.3.CO;2.

Sultan, M., Becker, R., Arvidson, R.E., Shore, P., Stern, R.J., El Alfy, Z., and Attia, R.I., 1993, New constraints on Red-Sea rifting from correlations of Arabian and Nubian Neoproterozoic outcrops: Tectonics, v. 12, p. 1303–1319, doi: 10.1029/93TC00819.

Sultan, M., Sturchio, N., Hassan, F.A., Hamdan, M.A.R., Mahmood, A.M., ElAlfy, Z., and Stein, T., 1997, Precipitation source inferred from stable isotopic composition of Pleistocene groundwater and carbonate deposits in the Western Desert of Egypt: Quaternary Research, v. 48, p. 29–37, doi: 10.1006/qres.1997.1907.

Sultan, M., Sturchio, N.C., Gheith, H., Hady, Y.A., and El Anbeawy, M., 2000, Chemical and isotopic constraints on the origin of Wadi El-Tarfa Ground Water, Eastern Desert, Egypt: Ground Water, v. 38, p. 743–751, doi: 10.1111/j.1745-6584.2000.tb02710.x.

Sultan, M., El Alfy, Z., Becker, R., Milewski, A., and Bufano, E., 2003a, A web-based GIS for Egypt's geologic datasets: Geological Society of America Abstracts with Programs, v. 35, p. 261.

Sultan, M., Flower, M., Becker, R., Milewski, A., Bufano, E., Sandvol, E., and Danishwar, S., 2003b, A preliminary dataset for the "Tethys" database: Geological Society of America Abstracts with Programs, v. 35, p. 261.

Sultan, M., Yan, E., Sturchio, N., Wagdy, A., Milewski, A., Abdel Gelil, K., Manocha, N., and Becker, R., 2007, Natural discharge: A key to sustainable utilization of fossil groundwater: Amsterdam, Journal of Hydrology, v. 335, p. 25–36, doi: 10.1016/j.jhydrol.2006.10.034.

Sultan, M., Sturchio, N., Al Sefry, S., Milewski, A., Becker, R., Nasr, I., and Sagintayev, Z., 2008a, Geochemical, isotopic, and remote sensing constraints on the origin and evolution of the Rub Al Khali aquifer system, Arabian Peninsula: Journal of Hydrology, v. 356, p. 70–83.

Sultan, M., Wagdy, A., Manocha, N., Sauck, W., Abdel Gelil, K., Youssef, A.F., Becker, R., Milewski, A., El Afry, Z., and Jones, C., 2008b, An integrated approach for identifying aquifers in transcurrent fault systems: The Najd shear system of the Arabian Nubian Shield: Amsterdam, Journal of Hydrology, v. 349, p. 475–488, doi: 10.1016/j.jhydrol.2007.11.029.

Telford, W.M., Geldart, L.P., and Sheriff, R.E., 1990, Applied Geophysics: Cambridge University Press, 770 p.

Vallée, M.A., Chouteau, M., and Palacky, G.J., 1992, Variations of the VLF-EM primary field: Analysis of airborne survey data: Geophysics, v. 57, p. 181–186, doi: 10.1190/1.1443182.

Vengosh, A., Hirschfeld, D., Vison, D., Dwyer, G., Raanan, H., Rimawi, G., Al-Zoubi, A., Akkawi, E., Marie, A., Haquin, G., Zaarur, S., and Ganor, J., 2009, High naturally occurring radioactivity in fossil groundwater from the Middle East: Environmental Science and Technology, v. 43, p. 1769–1775, doi: 10.1021/es802969r.

Wasfi, S., and Azazi, G., 1979, Stratigraphy of the northern Gulf of Suez: Annals of the Geological Society of Egypt, v. 9, p. 308–321.

Winn, R.D., Crevello, P.D., and Bosworth, W., 2001, Lower Miocene Nukhul formation, Gebel el Zeit, Egypt: Model for structural control on early synrift strata and reservoirs, Gulf of Suez: American Association of Petroleum Geologists Bulletin, v. 85, p. 1871–1890.

Younes, A.I., and McClay, K., 2002, Development of accommodation zones in the Gulf of Suez–Red Sea rift, Egypt: American Association of Petroleum Geologists Bulletin, v. 86, p. 1003–1026.

Manuscript Received 5 August 2009
Revised Manuscript Received 7 April 2010
Manuscript Accepted 13 April 2010

Printed in the USA